# Diffusion coefficients in anisotropic fluids by ESR imaging of concentration profiles[a)]

J. P. Hornak,[b)] J. K. Moscicki,[c)] D. J. Schneider, and J. H. Freed
*Baker Laboratory of Chemistry, Cornell University, Ithaca, New York 14853*

(Received 24 September 1985; accepted 6 December 1985)

We report on the use of ESR imaging for determining the translational diffusion constants of typical ESR spin probes in ordered and isotropic solvents. A discussion is given for a Fourier deconvolution method for determining the correct concentration profile if there is more than one hyperfine line in the spectrum of the radical as well as a spatial dependence of the spectrometer sensitivity. A simple but approximate subtraction deconvolution method is also presented. The diffusion constants for 4-oxo-2,2,6,6-tetramethylpiperidine-1-oxyl (TEMPONE) in the nematic and isotropic phases of the liquid crystal **p**-pentylbenzylidine-**p**-butylanaline (**5,4**) were determined. In the isotropic phase the diffusion coefficient is isotropic ($D = 2.5\times10^{-6}$ cm$^2$ s$^{-1}$, at 50 °C), while in the nematic phase it was found to be mildly anisotropic. The diffusion coefficients for motion perpendicular and parallel to the director axis in the nematic phase are respectively, $D_\perp = 9.0\times10^{-7}$ cm$^2$ s$^{-1}$, $D_\parallel = 6.4\times10^{-7}$ cm$^2$ s$^{-1}$ at 27 °C. This is interpreted in terms of some smectic-like character in the nematic phase of 5,4. Possible improvements in the technique are also discussed.

## I. INTRODUCTION

In the study of molecular dynamics in condensed media by ESR, there is need for a convenient technique for measuring translational diffusion coefficients $D$ for the spin probes. One can divide experiments designed to measure $D$ into two general categories: microscopic and macroscopic. A typical microscopic method used in ESR is the measurement of Heisenberg spin exchange (HSE) between colliding radical pairs. Line broadening due to such a method measures diffusion over dimensions on the order of molecular lengths.[1–3] The analysis leading to the diffusion coefficient depends upon the choice of the molecular model, a feature that is characteristic of microscopic methods in general. On the other hand, macroscopic methods, such as NMR field-gradient spin echoes, involve diffusion over macroscopic distances. These experiments may be interpreted in terms of the simple phenomenological description of diffusion to yield $D$.[4] One can employ a combination of microscopic and macroscopic measurements to better understand the details of molecular motions important for diffusion on all scales of distance.

Unfortunately, because the ESR time scale is so much faster than that of NMR, it is impossible to adapt the field-gradient spin-echo technique to determine condensed-phase diffusion coefficients less than $10^{-5}$ cm$^2$/s (see Ref. 42). On the other hand, one finds that an ESR-imaging approach may be utilized to measure $D$ of spin probes in liquids. The method is to prepare an ESR sample containing a nonequilibrium concentration distribution of spin probe and then to monitor the time evolution of the concentration profile. This is accomplished with the aid of a magnetic field gradient which introduces a linear dependence of the resonant fields on the position of the spin probe in the sample. We have found this approach to be very useful for measuring diffusion coefficients over a wide range of values ($10^{-5}$–$10^{-7}$ cm$^2$/s), and future improvements in technique are expected to increase the efficiency of the method and the range of $D$ convenient to study.

In this paper we describe our methods and our results with nitroxide probes in several solvents.[5] A similar technique has been outlined by Lebedev and co-workers[6] using other radicals. In particular, we describe in detail how Fourier deconvolution may be employed for obtaining the concentration profile and how one corrects for the varying sensitivity across the sample. Aside from our demonstration of the large range of values of $D$ which may be studied in liquids, we are also able to address a particularly important matter for liquid crystalline solvents viz. the anisotropy in the diffusion coefficient. NMR field-gradient spin-echo studies have already provided extensive evidence of anisotropy of $D$ in liquid crystalline phases.[7,8] We report the first measurement of anisotropic $D$ for a spin probe by an ESR imaging technique. Both the magnitude and the anisotropy of macroscopically measured diffusion coefficients are important both for discriminating between microscopic models of diffusion in liquid crystals and in models of molecular dynamics near the liquid crystalline phase transitions.[9–12] Experiments relying on HSE[9,10] cannot measure the anisotropy in macroscopic $D$ that is theoretically possible in these media.

We note that other macroscopic techniques employed to measure diffusion of spin probes and spin labels include that of Sheats and McConnell[13,14] which requires selective photobleaching of a sample and that of Ahn[15] which applies the capillary diffusion method[16] to ESR and requires a great deal of measurement time (e.g., about $10^6$ s for a

a) Supported by NSF Solid-State Chemistry Grant No. DMR-81-02047, by NSF Grant No. CHE-83-19826, and by NIH Grant No. GM-25862.
b) Present address: Department of Chemistry, Rochester Institute of Technology, Rochester, NY 14623.
c) Present address: Institute of Physics, Jagellonian University, ul. Remonta 4, 30-059 Cracow, Poland.

 0021-9606/86/063387-09$02.10  

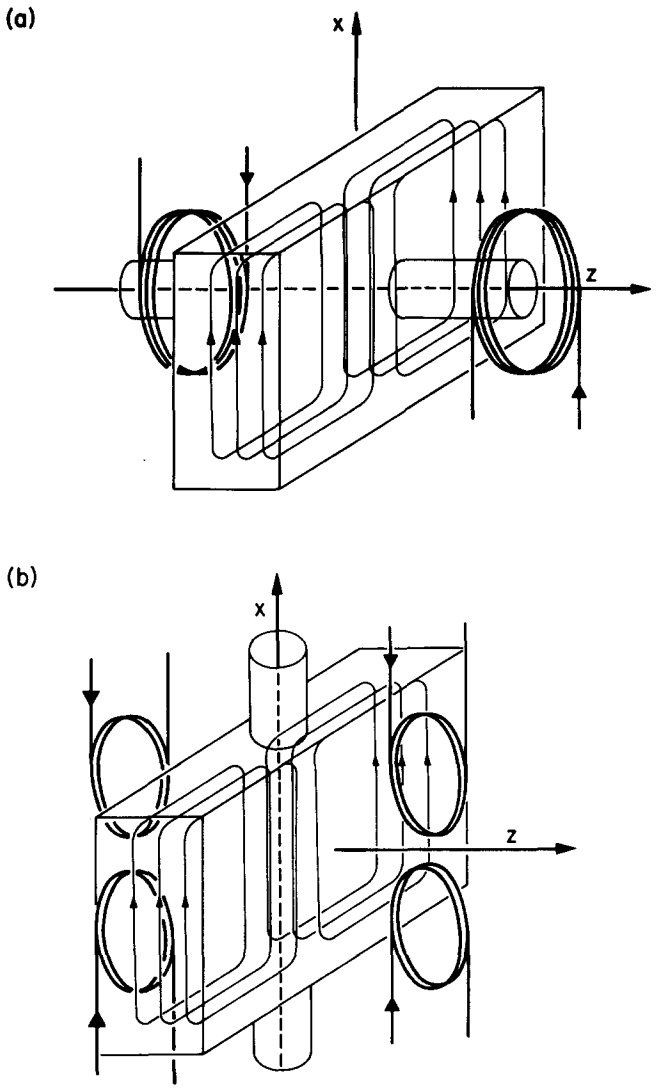


FIG. 1. Configuration of the (a) anti-Helmholtz, and (b) figure 8 coils which produce the static magnetic field gradients along the (a) $Z$ axis, and (b) $X$ axis, respectively, of a $TE_{102}$ $X$-band microwave cavity.

$D \sim 7 \times 10^{-6}$ cm$^2$/s). Other methods that have been used to measure translational diffusion coefficients in liquid crystals include radio-tracer, optical, and neutron scattering methods.[17–20] Also, other applications of ESR imaging[21–28] have included a measurement by Ohno[21] of rate constants of short lived radicals by a continuous flow method, while Hoch[27] investigated paramagnetic centers in diamonds, and Berliner[24] has been developing a technique to image living tissues.

In Sec. II we describe our experimental methods for ESR imaging of concentration profiles, while in Sec. III we discuss the deconvolution methods. The procedure for obtaining diffusion coefficients from the concentration profiles is outlined in Sec. IV, and our results are presented there. Discussion of these results and possible improvements in technique appears in Sec. V.

## II. EXPERIMENTAL METHODS

All ESR experiments reported here were performed at $X$ band on either a Varian model E12 or Bruker model ER-200D spectrometer. All spectra were recorded in the standard first derivative mode with 100 kHz modulation and microwave powers of about 10 mW.

Electron spin-resonance imaging was carried out inside a modified Varian $TE_{102}$ narrow flange $X$-band microwave cavity. One-dimensional images were recorded along the $X$ and $Z$ axes, respectively, of the cavity. Figure 1 shows the $TE_{102}$ cavity with the conventional $XYZ$ coordinate system, the microwave magnetic field, and the placement of the sample and field-gradient coils. Imaging along the $X$ axis utilized the standard Varian sample mounts and temperature controlling Dewar for the cavity [Fig. 1(a)]. However, modifications were made in the cavity for imaging along the $Z$ axis [Fig. 1(b)]. Observations in a gradient along the $Z$ axis required mounting a sample through the walls of the cavity parallel to the applied $H_0$. This was accomplished by modifying the cavity walls to contain two chimneys. The walls were constructed out of 0.102 mm thick brass sheets onto which 2.8 mm i.d. by 1.4 cm long brass cylinders were attached. These walls were silver plated and cemented to the modulation coils with the chimney passing through the center of the coil. The diameter and length of the chimneys were chosen so as to allow insertion of a temperature controlling quartz jacket. The quartz jacket was attached via a 90° elbow to the output of the standard Varian Dewar located below the cavity while preventing leakage of microwave radiation.

In our experiment, linear magnetic field gradients in the $H_0$ magnetization were employed. A gradient in $B_0$ along the $Z$ axis of the cavity was achieved by a set of coils placed on either side of the ESR cavity in anti-Helmholtz configuration [Fig. 1(a)]. A gradient in $H_0$ along the $X$ axis was achieved by a pair of "figure 8" coils [Fig. 1(b)]. The details of the coil geometries will be described next.

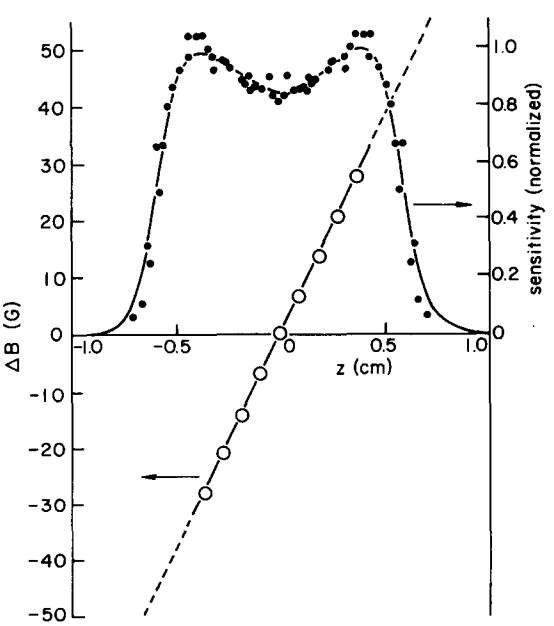


FIG. 2. Cavity sensitivity and field gradient along the $Z$ axis. Sensitivity (O) as a function of position along the $Z$ axis of the modified $TE_{102}$ cavity as determined from a small quantity of microcrystalline DPPH moved along the axis. The solid line through these points represents the sensitivity as determined by imaging (see the text). The magnetic field gradient along the $Z$ axis (O) as determined from a small quantity of microcrystalline DPPH moved along the $Z$ axis of the cavity. The straight line fit represents a gradient of 77 G/cm.

The coils producing the $Z$ gradient consisted of eight small equal diameter coils, four on either side of the cavity. These coils had as a common axis a line running through the center of the side walls of the cavity. Each of the small coils (i.d. = 2.2 cm, o.d. = 5.2 cm, width = 2.54 mm) contained approximately 500 turns of No. 30 Cu wire and were separated by approximately 1.27 mm. All coils were connected in parallel with the direction of the current being opposite on the two sides of the cavity. In this configuration the magnetic field as a function of $Z$ is $B(Z) = B_0 + B'_z(Z - \overline{Z})$ where $B_0$ is the magnetic field at the center of the cavity, $\overline{Z}$, and $B'_z$ the $Z$ component of the field gradient. Coils were wound on a plexiglass form with an epoxy adhesive. The plexiglass forms were mounted into two brass supports containing water cooling channels. The total resistance of the coils was 2.7 Ω (cold) and typically two A of current yielded a constant $B_0$ field gradient of 77 G/cm (see Fig. 2). (The gradient in $B_0$ radially from the $Z$ axis was approximately 0.4 G/cm with these coils.)

The problem of producing constant field gradients along the $X$ axis is more complex than along the $Z$ axis. To achieve this gradient two pairs of figure 8 coils were needed. Each pair was constructed to approximate the field in a long cylindrical coil. This geometry minimizes the gradient along the axis of the coil. The coils were mounted such that one pair covered the top half of the cavity and the other the bottom. The resultant magnetic field $B(X)$ is $B(X) = B_0 + B'_x(X - \overline{X})$ where $B'_x$ is the $X$ component of the field gradient (see Fig. 3). Each of the coils making up the pair was wound with 300 turns of No. 26 Cu wire. The turns were epoxied in place on a rectangular form of approximately 1.21 by 1.55 cm and 2.16 cm in length which was later removed. The coils were connected in series and had a total resistance (cold) of 10 Ω. Two A of current yielded an $X$ gradient of 60 G/cm. The coils were mounted on the side of the cavity and enclosed with a jacket which allowed cooling with 200 K nitrogen. This coil geometry minimizes annular thickness of the coils thus allowing the minimum space between the coils making up the figure 8 on each side, and minimizes the gradient along the $Y$ direction of the cavity.

Temperature control of samples oriented along the $Z$ axis was accomplished by directing the temperature regulated $N_2$ gas from the Varian variable temperature cavity Dewar through the quartz jacket. The temperature gradient in this orientation was less than 0.19 K/cm. Temperature control in both orientations was accomplished using the standard Varian temperature controlling unit. The long-term temperature stability in both geometries was ± 0.5 K and is limited by the stability of the Varian temperature controlling unit.

Since these experiments involve samples extending over the distance of the order of the wavelength of the irradiating microwave field, it is essential to determine the variation in the sensitivity of the spectrometer over the spatial dimensions of the sample. The sensitivity was measured directly by monitoring the amplitude of the signal obtained from a very small (about $10^{-6}$ cm$^3$) quantity of microcrystalline diphenyl picryl hydrazyl (DPPH) as a function of position in the cavity in the absence of magnetic field gradients. The

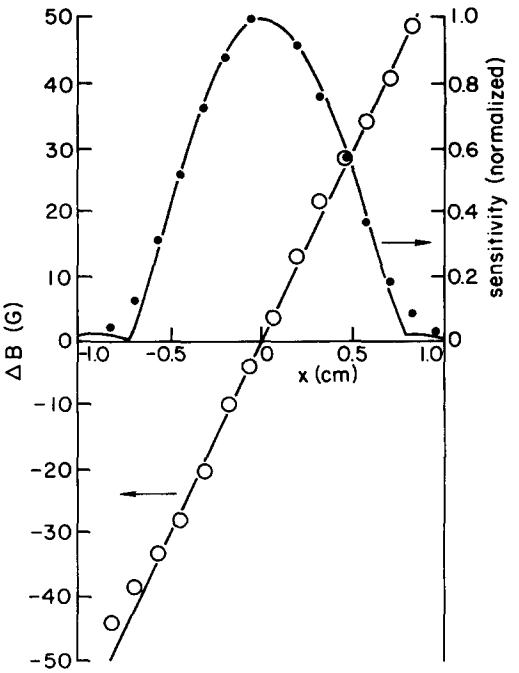


FIG. 3. Cavity sensitivity and field gradient along the $X$ axis. Sensitivity (O) as a function of position along the $X$ axis of the modified $TE_{102}$ cavity as determined by moving a small amount of microcrystalline DPPH along the axis. The solid line through these points represents the sensitivity as determined by imaging (see the text). The magnetic field gradient along the $X$ axis (O) as determined from a small amount of microcrystalline DPPH moved along the $X$ axis of the cavity. The straight line fit of the points represents a gradient of 60 G/cm.

DPPH was epoxied onto the end of a thin (about 0.01 cm diam) glass rod attached to a micrometer device for accurate determination of the position in the cavity. (It could also be measured by imaging methods as described below.)

The magnetic field gradient was measured in a similar manner. The magnetic field at which the maximum in the resonance line of the DPPH occurred was recorded as a function of the spatial position in the presence of the magnetic field gradient.

To prepare a sample that approximated diffusion from a point source, a capillary tube was filled with solvent, and a very small amount of spin probe (dissolved in the same solvent) was placed at one end. To avoid Heisenberg spin-exchange broadening of the lines in the region of observation, the point source was placed about 0.6 cm outside the cavity so that the spin-probe concentration in the cavity was always less than about 0.001 M. The presence of Heisenberg spin exchange would render our methods invalid.

Experiments were performed in this manner using the liquid crystal parapentylbenzylidene-p-butylaniline (**5,4**) (Frinton Labs, Inc.), and the spin probe was 4-oxo-2,2,6,6,-tetramethylpiperidine-1-oxyl (TEMPONE). The liquid crystal conveniently has a nematic phase between 298–303 K with an isotropic phase above 303 K and a smectic $C$ phase below 298 K (extending to 273 K). (Experiments on the normal liquids: $H_2O$ and ethanol were performed in a somewhat different sample arrangement that proved not to be as convenient.)

The nematic phase samples were aligned such that the

director axis was parallel to the main external field before spectra were recorded. This was accomplished by quickly raising the temperature above the nematic–isotropic transition point then cooling it in the presence of the external field. The sample was then held at a constant temperature of 300 K for the duration of the experiment. The samples in the $X$ orientation corresponded to diffusion perpendicular to the director axis and samples in the $Z$ orientation corresponded to diffusion parallel to the director axis. Independent experiments were performed to record the usual ESR spectrum in the absence of magnetic field and spin-probe concentration gradients, since this information is needed for the deconvolution of the concentration profiles (cf. Sec. III).

The spectra of TEMPONE in the isotropic phase solvent were recorded at 323 K in both the $X$ and $Z$ orientations. This was done to check the consistency of the method since the diffusion constant should not depend on orientation in an isotropic liquid.

The measured sensitivity (normalized relative to the maximum observed sensitivity) for the $Z$ orientation is shown in Fig. 2 and for the $X$ orientation in Fig. 3. The magnetic field gradient, determined with the DPPH crystal, is also shown in these figures. In both cases, the line through the open circles represents the best fit of a straight line to the magnetic field gradient data. The magnetic field gradient was determined to be 60 G/cm in the $X$ orientation and 77 G/cm in the $Z$ orientation. These gradients show very little deviation from linearity.

In both orientations the sensitivity strongly depends on the position in the cavity. An assumption that the sensitivity does not depend on the position in the cavity would lead to large deviations in the experimentally determined concentration profiles from the correct ones. A typical sensitivity curve obtained by using the subtraction deconvolution method (see Sec. III) on a sample with a uniform concentration profile is superimposed on the closed circles as a demonstration of the similarity of the results obtained with the DPPH and the deconvolution method.

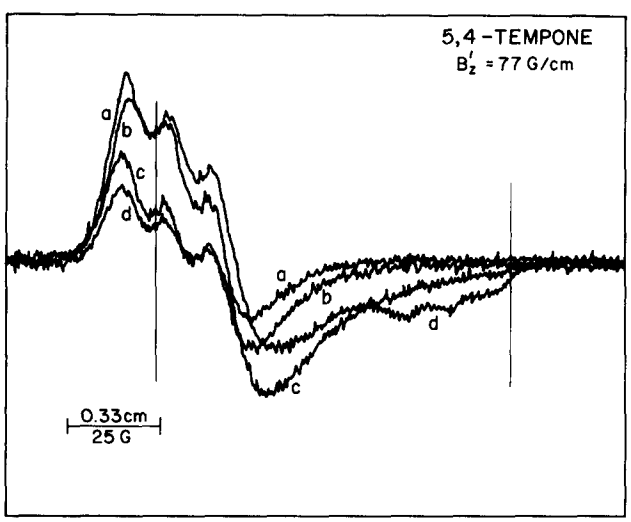


FIG. 4. A series of spectra from imaging concentration profiles along the $Z$ axis of the $TE_{102}$ cavity. The spectrum is a 200 G scan recorded in 2 min with a 77 G/cm gradient along the $Z$ axis. The concentration profile is from TEMPONE spin probe in the nematic phase of **5,4** diffusing from a point source at the left of the spectrum and in a direction parallel to the axis of alignment. The spectra were recorded at different relative times after the start of diffusion, (a) $t = 0$ s, (b) $t = 3.1\times10^4$ s, (c) $t = 2.1\times10^5$ s, and (d) $t = 5.0\times10^5$ s.

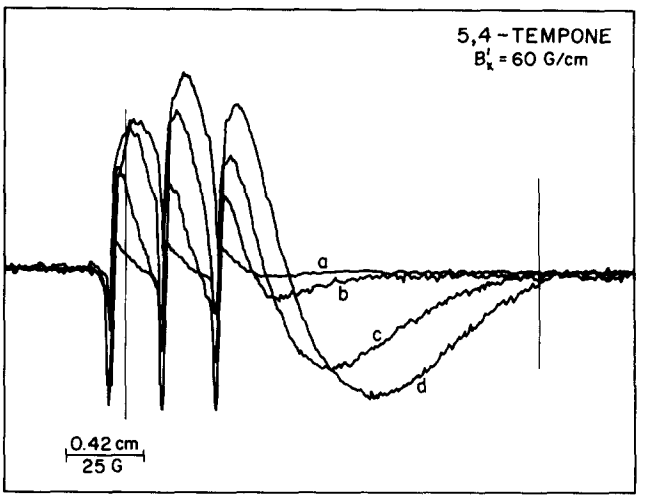


FIG. 5. A series of spectra from imaging concentration profiles along the $X$ axis of the $TE_{102}$ cavity. The spectrum is a 200 G scan recorded in 2 min with a 60 G/cm gradient along the $X$ axis. The concentration profile is from TEMPONE spin probe in the isotropic phase of **5,4** diffusing from a point source at the left of the spectrum. The spectra were recorded at different relative times after the start of diffusion, (a) $t = 0$ s, (b) $t = 1.2\times10^4$ s, (c) $t = 9.8\times10^4$ s, and (d) $t = 2.0\times10^5$ s.

A series of representative spectra showing the time evolution of the experimentally observed derivative mode signal from an initially nonequilibrium spin-probe concentration profile in the $Z$ orientation are shown in Fig. 4 and in the $X$ orientation in Fig. 5.

The derivative mode ESR spectra were digitized as they were recorded, then numerically integrated to give the absorption spectra needed for the deconvolution procedures described in Sec. III.

## III. DECONVOLUTION METHODS

The experiment was designed (see Sec. II) such that the linear magnetic field gradient is parallel to the concentration gradient. Thus the total magnetic field, $B(x)$, can be written as

$$B(x) = \overline{B} + B'(x - \bar{x}), \tag{3.1a}$$

where $\overline{B}$ is the strength of the magnetic field at the center of the cavity, $x = \bar{x}$, and $B' = dB/dx$. Here, $x$ denotes the distance in the cavity in either of the two experiments. For simplicity in the following sections, we define new variables $y = \overline{B} - B'\bar{x}$ and $\beta = -B'$. The relation for $B(x)$ is then

$$B(x) = y - \beta x. \tag{3.1b}$$

### A. Fourier deconvolution

The absorption spectrum, $I_g(B,t)$, in the presence of magnetic field and concentration gradients can be expressed as the convolution of the absorption spectrum in the absence of concentration and magnetic field gradients, $I_0(B)$, with the product $S(x)c(x,t)$, where $S(x)$ is the sensitivity per unit concentration as a function of the spatial coordinate. It

should also be noted that this expression is only valid in the absence of Heisenberg spin-exchange (HSE) broadening, since HSE effects would vary across the sample due to their concentration dependence.

Using Eq. (3.1b) the convolution expression for $I_g(y,t)$ can be written as

$$I_g(y,t) = \int_{-\infty}^{\infty} g(x,t) I_0(y - \beta x) dx, \tag{3.2}$$

where $g(x,t) = S(x)c(x,t)$ is the "effective concentration" function. The expression for $I_g(y,t)$ has the obvious physical interpretation as the superposition of the signals of individual spin probes at different positions weighted by the spectrometer sensitivity at that position.

The problem of analyzing the experimental data is to invert this integral equation to give $c(x,t)$ in terms of the experimentally measurable quantities $S(x)$, $I_0(B)$, and $I_g(B,t)$. This task can be most easily accomplished by using the fact that the Fourier transform of a convolution of two well behaved functions is the product of the Fourier transforms of the individual functions. Taking the Fourier transforms of both sides of Eq. (3.2) with respect to $y$ gives

$$\tilde{I}_g(k,t) = \tilde{g}(k\beta,t)\tilde{I}_0(k). \tag{3.3}$$

Dividing both sides of Eq. (3.3) and performing the inverse Fourier transform yields the required relation for $g(y/\beta,t)$,

$$g(y/\beta,t) = \frac{-B'}{2\pi} \int_{-\infty}^{\infty} e^{+iky} \frac{\tilde{I}_g(k,t)}{\tilde{I}_0(k)} dk, \tag{3.4}$$

which is identical to $g(x,t)$. The function $S(x)$ can be determined from a separate experiment in which the capillary contains a uniform concentration of spin probe in the same solvent.

The experimental data was actually analyzed in the following manner. A pair of experimental runs obtained under similar conditions, were recorded for each time. One was taken with the field gradient on; the second was taken with the field gradient off. These were numerically integrated by standard methods to give $I_g(B,t)$ and $I_0(B)$, respectively. Second, these integrated spectra were subject to a fast Fourier transform (FFT) to give $\tilde{I}_g(k,t)$ or $\tilde{I}_0(k)$, respectively. Third, the inverse FFT of the quotient of the transformed spectra was done in a special manner to avoid numerical problems. If $\tilde{I}_0(k)$ was on the order of the unit round-off error of the computer for some values of $k$, then division by that value gave a result that was highly dependent on the accumulation of errors in the computation. A modification of the Wiener filter concept[29] was implemented to filter out this numerical "noise." The modified Wiener filter consisted of multiplying the integrand of Eq. (3.4) by a filtering function $W(k)$,

$$W(k) = \frac{|\tilde{I}_g(k,t)|^2}{|\tilde{I}_g(k,t)|^2 + u}, \tag{3.5}$$

where $u$ is a small positive constant on the order of the unit round-off error. This function acted as a filter by forcing the integrand of Eq. (3.4) to very small values wherever $I_g(k,t)$ has small magnitudes, regardless of the magnitude of $I_0(k)$, thus removing those areas most corrupted by numerical errors. With this filter function we have an approximate expression for $g(x,t)$ given by

$$g(x,t) = \frac{-B'}{2\pi} \int_{-\infty}^{\infty} e^{-iky} \frac{\tilde{I}_g(k,t)}{\tilde{I}_0(k)} W(k)\, dk. \tag{3.6}$$

The results obtained using Eq. (3.6) were quite insensitive to the choice of the magnitude of $u$, but omitting it altogether caused floating point overflows and other errors. Finally, the concentration profile was obtained. The sensitivity function $S(x)$ was first determined using Eq. (3.6) for the particular spin probe–solvent system and gradient coil placement. The resonant properties of the cavity can be altered by the introduction of the capillary, especially if it contains an aqueous sample, so it was important to use the sensitivity curve obtained in this fashion rather than the one measured with the DPPH in the deconvolution procedure. The concentration profile was then obtained by dividing $g(x,t)$ by $S(x)$.

### B. Approximate deconvolution by subtraction

In certain instances, it was useful to be able to quickly obtain an approximate concentration profile. This procedure, which we refer to as the subtraction deconvolution, is similar to the method of Brumby.[30] It was assumed that the spectrum in the absence of gradients $I_0(\bar{B})$ can be written as a sum of three hyperfine lines, all with the same shape,

$$I_0(\bar{B}) = a_1 J(\bar{B} - B_1) + a_2 J(\bar{B}) + a_3 J(\bar{B} + B_3), \tag{3.7}$$

where the $a_i$'s are the intensities of the individual hyperfine components and $B_i$'s are the offsets relative to the central line, and $J(B)$ is the line shape function. If this assumption is valid, the convolution integral describing the line shape can be expressed as a sum of three separate terms,

$$\begin{aligned} I_g(\bar{B},t) = a_1 &\int_{-\infty}^{\infty} g(x,t)\, J[\bar{B} - B_1 - B'(x - \bar{x})]dx \\ + a_2 &\int_{-\infty}^{\infty} g(x,t)\, J[\bar{B} - B'(x - \bar{x})]dx \\ + a_3 &\int_{-\infty}^{\infty} g(x,t)\, J[\bar{B} + B_3 - B'(x - \bar{x})]dx. \end{aligned} \tag{3.8}$$

All three terms on the right-hand side of Eq. (3.8) have the same functional form (i.e., exhibit the same dependence on $\bar{B}$). Thus, as long as the offsets are much greater than the widths of the hyperfine components, it is easy to subtract off the contributions of two of the three lines. Now, if the width of $J(B)$ is much less than that of $g[B(x),t]$ [cf. Eq. (3.8)], then $J(B)$ can be approximated as a delta function in the integrands of Eq. (3.8), so the subtracted $I_g(\bar{B},t)$ is a good approximation to $g[B(x),t]$. Thus, under these conditions Fourier deconvolution would not be necessary.

The subtraction deconvolution procedure was used to analyze the experimental data with negligible hyperfine peak overlap. It can be summarized as follows: First, the peak heights of each of the hyperfine lines ($a_i$) and the separation of the lines ($B_i$) were determined from the maxima in the integrated spectra. Secondly, an approximate $g(x,t)$ was calculated by proceeding from low field to high field and subtracting off the contributions of the middle and high field lines from the experimental diffusion ESR spectra. We found that due to slight additive errors in this technique it

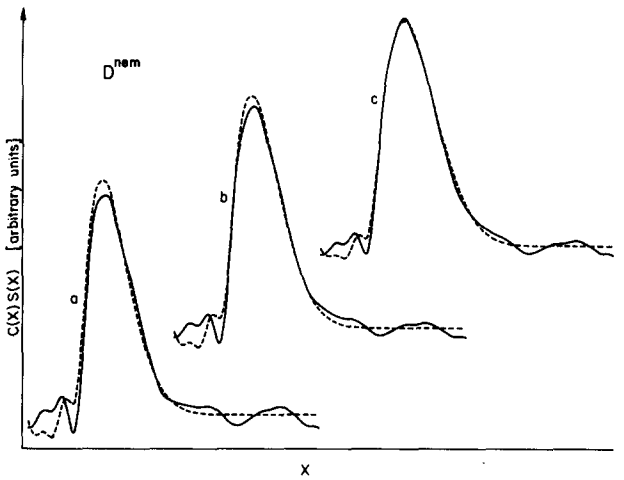


FIG. 6. Concentration profile times $X$-axis cavity sensitivity (–) for TEMPONE diffusing in the nematic phase of 5,4 at 300 K deconvoluted from the ESR spectra using the Fourier transform technique (see the text). These three curves were recorded at different relative times (a) $2.2\times10^4$ s, (b) $9.7\times10^4$ s, and (c) $1.56\times10^5$ s after the start of diffusion. The broken lines are the linear least square fit of the data obtained by multiplying the cavity sensitivity along the $X$ axis times the calculated concentration assuming diffusion from a point source with $Dt$ equals (a) $9.32\times10^{-2}$, (b) 0.142, and (c) 0.93 cm$^2$.

was necessary to average with this a spectrum with the effects of the low field and middle lines subtracted off by proceeding from high field to low field. The last step was to assume a diffusion coefficient to insert into $h(x,t)$, Eq. (4.5). The diffusion constant was empirically varied to minimize the deviations of $h(x,t)$ from the approximate $g(x,t)$. This manual fitting procedure consistently gave a very good fit to the data by comparison with the more rigorous Fourier deconvolution method.

## IV. DIFFUSION COEFFICIENTS FROM CONCENTRATION PROFILES

Our analysis is based on the assumption that the concentration of spin probe is low enough that the translational diffusion obeys Fick's Law[31]:

$$\frac{\partial C(x,t)}{\partial t} = D\frac{\partial^2 C(x,t)}{\partial x^2}. \tag{4.1}$$

If the initial distribution of spin probe is close to that of a delta function at $x=0$ we may use

$$C(x,t=0) = C_0\delta(x); \tag{4.2}$$

then a simple solution to Eq. (4.1) exists as[31(a)]

$$C(x,t) = [C_0/(4\pi Dt)^{1/2}]e^{-x^2/4Dt}, \tag{4.3}$$

where we have used the boundary condition that $\partial C/\partial x|_{x=0} = 0$, corresponding to a reflecting wall at $x=0$, and we have ignored the other boundary at $x=L$, since in our experiments the spin probe never reaches it.

More generally for an arbitrary initial distribution of spin probes (neglecting for simplicity any boundary effects) one may first write down the Green's function and thus obtain the solution[31(b)]

$$C(x,t) = \frac{1}{(4\pi Dt)^{1/2}}\int_{-\infty}^{\infty} e^{-(x-x')^2/4Dt}C(x',t=0)dx'. \tag{4.4}$$

[Equation (4.4) may, of course, be adapted to any specific boundaries such as reflecting walls at $x=0$ and $L$,[31(b)] without significant change in the qualitative nature of its discussion given below.]

Utilizing these expressions, the diffusion coefficient may be obtained from a series of experimentally measured $g(x,t)$ for different $t$ and the associated $S(x)$. For the case we used, i.e., the initial "point source" approximation, it is con-

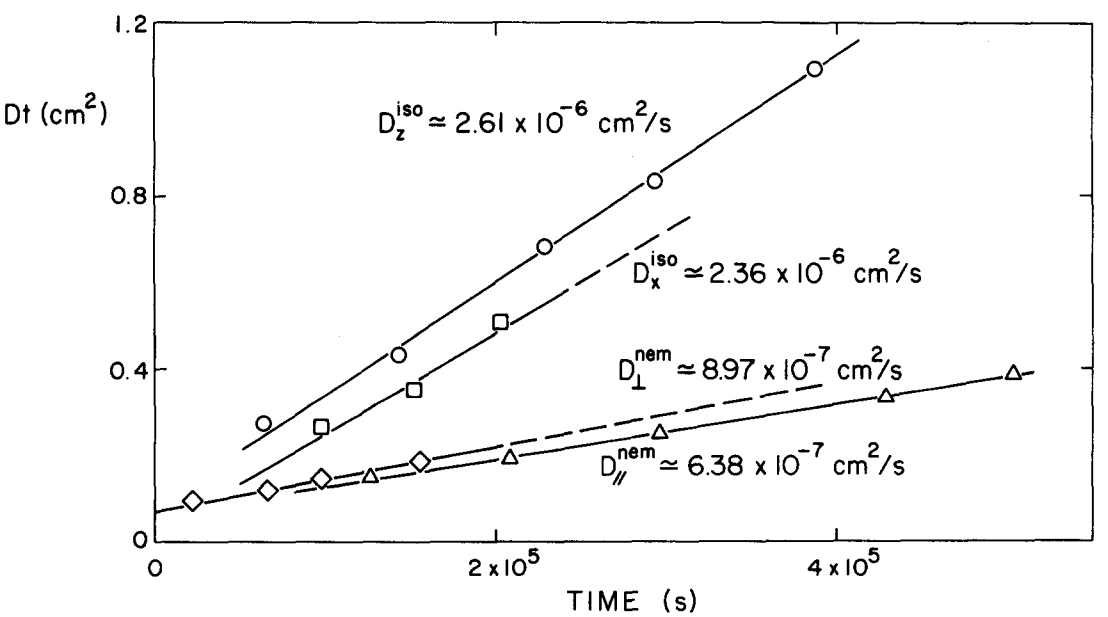


FIG. 7. A plot of $Dt$ (cm$^2$) values calculated by the Fourier transform technique (see the text) as a function of time for TEMPONE diffusing through 5,4. The phase and direction of the impurity diffusion in the liquid crystal are (○) isotropic and $Z$ axis, (□) isotropic and $X$ axis, (△) nematic and parallel, and (◇) nematic and perpendicular. The solid lines are a linear least squares fit to the points with $D$ equal to (○) $2.61\times10^{-6}$, (□) $2.36\times10^{-6}$, (◇) $8.97\times10^{-7}$, and (△) $6.83\times10^{-7}$ cm$^2$ s$^{-1}$. The calculated ratio value of $D_{\parallel}$ to $D_{\perp}$ is 0.71.

venient to introduce a new "effective concentration" function, $h(x,t)$, defined by

$$h(x,t) = [S(x)C_0/(4\pi Dt)^{1/2}]e^{-x^2/4Dt}, \quad (4.5)$$

which should closely approximate $g(x,t)$. Dividing $g(x,t)$ by $h(x,t)$ and taking the logarithm gives the useful relation:

$$\ln\frac{g(x,t)}{h(x,t)} = \ln[C(x,t)] + x^2/4Dt - \ln[C_0/(4\pi Dt)^{1/2}]. \quad (4.6)$$

Using this equation, the quantities $(1/4Dt)$ and $\ln[C_0/(4\pi Dt)^{1/2}]$ were determined by standard least-square minimization (with respect to the independent variable $x^2$) for each of the spectra taken at the different times. Typical fits of $h(x,t)$ to $g(x,t)$ for diffusion along the $X$ axis obtained with this method of data analysis are shown in Fig. 6. The diffusion constant was then obtained from the limiting slope at long times of the plot of $Dt$ vs $t$.

Such plots, obtained using the Fourier deconvolution method, are shown in Fig. 7. Some curvature in the plots shown in Fig. 7 are observable at short times. This could be attributed to deviations from true delta function boundary conditions at zero elapsed time due to sample preparation or alignment procedure. [Any deviations of this type should be unimportant after a time on the order of $(\Delta x)^2/D$ where $\Delta x$ is the finite width of the initial distribution of spin-probe concentration.] The more general approach using the Green's function method of predicting the time evolution of the concentration profile (see below) would not encounter these difficulties.

The estimates of $C_0$ were found to be equal for all members of a given series of spectra, as they should be. The diffusion constant for TEMPONE in the isotropic phase of **5,4** was found to be isotropic to within experimental error (about 5%–10%), ($D_\perp = 2.4\times10^{-6}$ cm$^2$ s$^{-1}$, $D_\parallel = 2.6\times10^{-6}$ cm$^2$ s$^{-1}$) as expected. The diffusion constants for motion perpendicular and parallel to the director axis in nematic phase were found to be mildly anisotropic ($D_\perp = 9.0\times10^{-7}$ cm$^2$ s$^{-1}$, $D_\parallel = 6.4\times10^{-7}$ cm$^2$ s$^{-1}$). This gives a ratio of $D_\parallel/D_\perp$ equal to $0.71 \pm 0.1$ for the nematic phase (and $1.08 \pm 0.1$ for the isotropic phase).

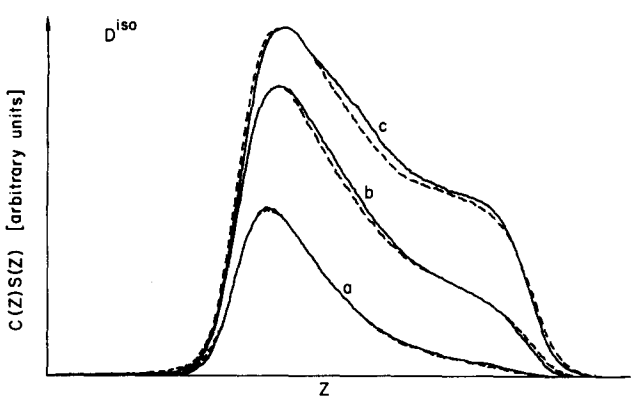


FIG. 8. Concentration profile times $Z$-axis cavity sensitivity (–) for TEMPONE diffusing in the isotropic phase **5,4** at 323 K deconvoluted from the ESR spectra using the subtraction technique (see the text). These three curves were recorded at different relative times (a) $3.64\times10^4$ s, (b) $1.44\times10^5$ s, and (c) $2.94\times10^5$ s after the start of diffusion. The broken lines are the best fit of the data obtained by multiplying the cavity sensitivity along the $Z$ axis times the calculated concentration assuming diffusion from a point surface with $Dt$ equals (a) 0.29, (b) 0.53, and (c) 0.90 cm$^2$.

TABLE I. Translational diffusion coefficients measured by ESR imaging.

| Solvent | Probe | Temperature (K) | $D$(cm$^2$ s$^{-1}$) |
|---|---|---|---|
| $H_2O$ | TEMPONE | 295 | $1.7\times10^{-5}$ |
| $C_2H_5OH$ | 2,5DTBSQ[a] | 295 | $2.7\times10^{-5}$ |
| **5,4** (iso) | TEMPONE | 323 | $2.5\times10^{-6}$ |
| **5,4** (nem)$D_\perp$ | TEMPONE | 300 | $9.0\times10^{-7}$ |
| **5,4** (nem)$D_\parallel$ | TEMPONE | 300 | $6.4\times10^{-7}$ |

[a] 2,5 di-tertiary-butyl-para-benzosemiquinone.

One may generalize Eqs. (4.5) and (4.6) to produce a method for obtaining $D$ when the assumption of a point source is not made, so that an expression such as Eq. (4.4) is needed. One first obtains $C(x,t) = g(x,t)/S(x)$ for the concentration profile at each $t$. The Fourier transforms of these curves yield $\tilde{C}(k,t)$. The Fourier transform of Eq. (4.4) yields a predicted

$$\tilde{C}_p(k,t) = [e^{-k^2Dt}]\tilde{C}(k,0). \quad (4.7)$$

Then taking the log of $\tilde{C}(k,t)/\tilde{C}_p(k,t)$ gives

$$\ln\frac{\tilde{C}(k,t)}{\tilde{C}_p(k,t)} = 0 = \ln\frac{\tilde{C}(k,t)}{\tilde{C}(k,0)} + k^2Dt. \quad (4.8)$$

Thus, a least-squares analysis of the Fourier-transform concentration profile at each time $\tilde{C}(k,t)$ yields $Dt$. For this method the initial distribution $\tilde{C}(k,t=0)$ needs to be accurately determined by imaging (to within a constant factor), but one is free to choose as the $t=0$ concentration profile any one that is convenient to obtain.

We also used the approximate subtraction deconvolution procedure to determine the diffusion coefficients. Representative fits of $h(x,t)$ to $g(x,t)$ for diffusion along the $x$ axis are displayed in Fig. 8. The diffusion constant for TEMPONE in the isotropic phase of **5,4** is isotropic to within experimental error ($D_\perp = 2.2\times10^{-6}$ cm$^2$ s$^{-1}$, $D_\parallel = 2.4\times10^{-6}$ cm$^2$ s$^{-1}$), while those for the nematic phase are mildly anisotropic ($D_\perp = 7.3\times10^{-7}$ cm$^2$ s$^{-1}$, $D_\parallel = 5.3\times10^{-7}$cm$^2$ s$^{-1}$). This gives a ratio of $D_\parallel/D_\perp$ equal to $0.73 \pm 0.1$ for the nematic phase (and $1.09 \pm 0.1$ for the isotropic phase).

The two deconvolution techniques give comparable results in the cases studied here. However, at lower temperatures where the high field hyperfine line is substantially broader than the other two, the subtraction deconvolution method would not be applicable but the Fourier deconvolution method would be. For spin probes other than nitroxides, or for smaller field gradients, the assumption that the linewidth is much less than the difference in magnetic field over which the concentration changes might break down and render the subtraction deconvolution procedure invalid.

A summary of the translational diffusion coefficients that we have measured by ESR imaging appears in Table I.

## V. DISCUSSION

### A. Diffusion coefficients

A primary objective of this work was to demonstrate the feasibility and reliability of ESR imaging for measuring diffusion coefficients of nitroxide spin probes in a variety of solvents. Our results clearly demonstrate this. The results for spin probes in ordinary liquids are consistent with values obtained from HSE measurements for similar cases[1–3,32,33] and further studies would permit detailed comparisons to extract from the HSE results such microscopic parameters as the effective range of the exchange interactions.[1,3,34]

Of particular interest, has been the demonstration of how ESR imaging could yield the anisotropy ratios $D_{\parallel}/D_{\perp} = 0.7$ in the nematic phase of **5,4**. The reliability of our method is confirmed in that this ratio is found to be unity, within experimental uncertainty, for the isotropic phase despite important differences in the experimental details of measuring $D_{\parallel}$ and $D_{\perp}$. Again we note that our observed values of $D$ in a liquid crystal are of the order of those obtained for the probe TEMPONE in similar liquid crystals from HSE results[10,33,43] and more detailed comparisons of results for identical systems would be useful for analysis of microscopic models. However, an important point to be made is that HSE results are incapable of providing the tensor components of $D$, while the macroscopic ESR imaging approach has succeeded in this.

The observation that $D_{\parallel}/D_{\perp} < 1$ is itself an interesting one. In general, studies on self-diffusion and impurity diffusion in the nematic phase, yield $D_{\parallel}/D_{\perp} > 1$, i.e., diffusion parallel to the director is slightly more rapid than diffusion in the perpendicular direction.[7,8] For solute molecules that are smaller than those of the liquid crystalline solvent, this is interpreted as due to the substantial orientational alignment of the larger somewhat rod-like, liquid crystal molecules which therefore provide more hindrance to diffusion in the directions normal to their direction of alignment. However Moseley and Lowenstein (ML)[8] have shown (by NMR field-gradient spin-echo methods) that when the liquid crystal has a lower lying smectic phase, then in some cases one will observe a $D_{\parallel}/D_{\perp} < 1$ in the nematic phase. This is interpreted as a pretransitional effect. In the smectic phases, in general, $D_{\parallel}/D_{\perp} \ll 1$, because the smectic layering leads to increased packing of the central aromatic core regions of the smectic layer which hinders motion perpendicular to this smectic layer (i.e., motion parallel to the nematic director). In the nematic phase above such a smectic phase there can be pretransitional short-range smectic layering which can similarly affect diffusion. Clearly, in such nematic phases the "nematic effect" and the "smectic effect" will be competing. Judging from cases studied by NMR, ML suggests that probes which tend to be expelled into the aliphatic chain region of the layers (as the temperature is lowered) may be the best candidates for a dominance of the smectic effect for which $D_{\parallel}/D_{\perp} < 1$. In previous ESR studies with TEMPONE in the benzylidene liquid crystals **40,6** and **40,8** that are closely related to **5,4** it was shown that TEMPONE exhibits this expulsion effect in the smectic phase.[35,36] In fact the notion that $D_{\parallel}$ is suppressed relative to $D_{\perp}$ as the nematic–smectic phase transition is approached has been invoked to help explain critical anomalies observed in the spin relaxation of TEMPONE at this phase transition.[12] The observation that $D_{\parallel}/D_{\perp} < 1$ in **5,4** is supportive of this, but clearly more detailed studies are in order. The main point remains that the ESR imaging method permits such studies.

### B. Improvements in techniques

We now wish to address matters pertaining to the applicability of this method of determining diffusion coefficients by ESR imaging. We have measured $D$ in the range of $\sim 5\times 10^{-7}$–$2\times 10^{-5}$ cm$^2$/s. For smaller $D$, the methods we have used require rather long periods of measurement based on allowing the diffusion process to proceed to at least 80% of completion (cf. Fig. 7 for $D \sim 10^{-6}$ cm$^2$/s). While this can become a significant problem for slower rates of diffusion, we note that the technique of ESR imaging to measure diffusion is in its infancy and there are many ways to improve it.

A significant improvement in the technique would be to set up an arbitrary initial concentration profile completely within the cavity and monitor it continuously. The time evolution of the concentration profile can then be predicted using the Green's function method, Eq. (4.4).

Such an experiment can be analyzed easily for a simple model case in which the initial concentration profile is Gaussian (with half-width: $\delta$ cm), if we also assume a single unsaturated Gaussian ESR line (with half-width: $\Delta$ G) such as can result from a single nitroxide hyperfine component that is inhomogeneously broadened by extensive proton superhyperfine structure.[37] One may then readily solve Eq. (4.4), and substitute this result into Eq. (3.2) taking $S(x) = 1$ (e.g., a loop-gap resonator, see below). Both integrals are just convolutions of Gaussians, and the result for $I_g(B,t)$ is just a Gaussian of width $\Gamma(t) = [\Delta^2 + \delta^2 B'^2 + DtB'^2]^{1/2}$. Now $B'$ should be chosen so as to maximize the fractional change in $\Gamma(t)$ at early times due to the diffusion, in order to optimize the experiment for slower diffusion. That is we wish to maximize

$$f \equiv \frac{1}{\Gamma^2}\frac{d\Gamma^2}{dt} = DB'^2/\Gamma(t)^2,$$

(where we have used the width squared purely for convenience). One immediately observes that $f$ is a maximum at $t = 0$ (for $B'^2 > 0$). Also, it is maximized by $B'^2 \gg \Delta^2/(\delta^2 + Dt)$. However, as larger field gradients are employed, $\Gamma$ can get very large, thereby spoiling the signal-to-noise ratio (S/N). Let us take $\mathrm{S/N} = A/\Gamma$, where $A$ is a quantity determined by the spectrometer conditions.[38] Ideally, we would like to simultaneously optimize $f$ and S/N to enable large fractional changes in the signal with diffusion while maintaining good S/N. We will for simplicity, just optimize the product $(\mathrm{S/N})^2 f$ (the square of S/N is used in recognition of the definition of $f$, above). One finds that this product is optimized by $B'^2 = \Delta^2/[\delta^2 + Dt]$, which enables us to obtain a rough estimate for the optimum $B'$.[44] (If S/N considerations are less important, then a correspondingly larger value of $B'$ could be used.) This leads to an optimum initial width, $\Gamma(t = 0) = \sqrt{2}\Delta$.

Now, if data are taken continuously, it should not be necessary to proceed beyond the time, $t_2$ such that

$\Gamma(t_2) = 2\Gamma(t=0)$. Then we obtain $t_2 = 3(\delta^2 B'^2 + \Delta^2)/DB'^2$, which becomes, using the optimum $B'$ obtained above (for $t=0$) $t_2 = 6\delta^2/D$. These expressions emphasize the importance of keeping the initial concentration profile narrow (i.e., $\delta$ small).

However, we would require that the maximum concentration in the initial profile, $C_{\max} < 10^{-3}$ M for a nitroxide spin probe in a typical liquid crystal to avoid the effects of HSE. We take as the minimum number of nitroxide spins required for *accurate line shape* measurements $N_{\min}$ as about $10^{15}$ spins[39] [on the assumption that $\Gamma(t=0)$ is the optimum value obtained above]. Then we have $\delta_{\min} = N_{\min}/\sqrt{2\pi} C_{\max} \pi r^2$ for our initial Gaussian distribution of spins along the length of a cylindrical sample of radius $r$. Letting $r \approx 0.25$ cm, we obtain $\delta_{\min} = 3.4 \times 10^{-3}$ cm. In actual experiments one usually has broader concentration profiles than this, so we can generally expect good signal-to-noise ratios.

If we then let $\delta \sim 0.1$ cm, we obtain $t_2 \sim 0.06/\mathrm{D}$ s. Thus a diffusion coefficient of $10^{-6}$ cm$^2$/s could be determined in no more than about 10–15 h instead of the six d taken in our present set of experiments. This result would scale linearly with $\mathrm{D}^{-1}$ for slower diffusion coefficients.

Also, one should employ a loop-gap resonator to increase the filling factor[40] of the very small samples needed to determine the small diffusion constants and to eliminate the cavity sensitivity function from the calculations.[41]


[1] M. P. Eastman, R.G. Kooser, M. R. Das, and J. H. Freed, J. Chem. Phys. **51**, 2690 (1969).
[2] J. C. Lang, Jr. and J. H. Freed, J. Chem. Phys. **56**, 4103 (1972).
[3] Y. N. Molin, K. M. Salikhov, and K. K. Zamaraev, *Spin-Exchange Principles and Applications in Chemistry and Biology* (Springer, New York, 1980).
[4] A. Abragam, *Principles of Nuclear Magnetism* (Oxford, New York, 1961).
[5] A preliminary account of this work was presented at the 7th International EPR Symposium, Rocky Mt. Conference, Denver, CO (Abstracts, August 1984).
[6] E. U. Galtzeva, O. Ye. Yakimchenko, and Ya. S. Lebedev, Chem. Phys. Lett. **99**, 301 (1983).
[7] G. J. Kruger, Phys. Lett. **82**, 229 (1982).
[8] M. E. Moseley and A. Loewenstein, Mol. Cryst. Liq. Cryst. **90**, 117 (1982).
[9] B. L. Bales, J. A. Swenson, and R. N. Schwartz, Mol. Cryst. Liq.Cryst. **28**, 143 (1974).
[10] A. Nayeem, V. S. S. Sastry, and J. H. Freed (to be published).
[11] J. H. Freed, J. Chem. Phys. **66**, 4183 (1977).
[12] S. A. Zager and J. H. Freed, Chem. Phys. Lett. **109**, 270 (1984).
[13] J. R. Sheats and H. M. McConnell, Proc. Natl. Acad. Sci. U. S. A. **75**, 4661 (1979).
[14] J. R. Sheats, Ph.D. dissertation, Stanford University, Stanford, CA, 1978.
[15] M. Ahn, J. Magn. Reson. **22**, 289 (1976).
[16] J. H. Wang, J. Am. Chem. Soc. **73**, 510 (1951).
[17] F. Rondelez, Solid State Commun. **14**, 815 (1974).
[18] H. Hakemi and M. M. Labes, J. Chem. Phys. **61**, 4020 (1970).
[19] C. K. Yun and A. G. Fredrickson, Mol. Cryst. Liq. Cryst. **12**, 73 (1970).
[20] H. Hakemi and M. M. Labes, J. Chem. Phys. **63**, 3708 (1975).
[21] K. Ohno, J. Magn. Reson. **49**, 56 (1982).
[22] K. Ohno, J. Magn. Reson. **50**, 145 (1982).
[23] M. J. R. Hoch, J. Phys. Chem. Solid State Phys. **14**, 5659 (1981).
[24] H. Fujii and L. J. Berliner, 7th International EPR Symposium, Rocky Mt. Conference, Denver, CO (August 1984).
[25] T. Herrling, N. Klimes, W. Karthe, U. Ewert, and E. Ebert, J. Magn. Reson. **49**, 203 (1982).
[26] S. S. Eaton and G.R. Eaton, J. Magn. Reson. **59**, 474 (1984).
[27] M. J. R. Hoch and A. R. Day, Solid State Commun. **30**, 211 (1979).
[28] W. Karthe and E. Wehrsdorfer, J. Magn. Reson. **33**, 107 (1979).
[29] R. C. Gonzales and P. Wintz, *Digital Image Processing* (Addison–Wesley, Reading, MA, 1977).
[30] S. Brumby, J. Magn. Reson. **34**, 317 (1979).
[31] (a) J. Crank, *The Mathematics of Diffusion*, 2nd ed. (Oxford University, Oxford, 1975); (b) P. M. Morse and H. Feshbach, *Methods of Theoretical Physics* (McGraw–Hill, New York, 1953).
[32] J. P. Hornak, Ph.D. thesis, University of Notre Dame, 1982.
[33] L.L. Jones and R. N. Schwartz, Mol. Phys. **43**, 527 (1981).
[34] (a) J. H. Freed, in *Chemically-Induced Magnetic Polarization*, edited by L. T. Muus *et al.* (Reidel, Dordrecht, 1977), Chap. 19; (b) G. P. Zientara and J. H. Freed, J. Phys. Chem. **83**, 3333 (1979).
[35] W. J. Lin and J. H. Freed, J. Phys. Chem. **83**, 379 (1979).
[36] E. Meirovitch, D. Igner, E. Igner, G. Moro, and J. H. Freed, J. Chem. Phys. **77**, 3915 (1982).
[37] B. L. Bales, J. Magn. Reson. **48**, 418 (1982).
[38] C. P. Poole, Jr., *Electron Spin Resonance* (Interscience, New York, 1967), p. 545.
[39] S. A. Zager, Ph.D. thesis, Cornell University, 1982; A. Nayeem, Ph.D. thesis, Cornell University, 1985.
[40] W. Froncisz and J. S. Hyde, J. Magn. Reson. **47**, 515 (1982).
[41] J. P. Hornak and J. H. Freed, J. Magn. Reson. **62**, 311 (1985).
[42] The problem with $D < 10^{-5}$ cm$^2$/s is as follows. Diffusion in the presence of a field gradient leads to an echo-envelope decay from a simple Hahn sequence given by $S(\tau) \propto \exp[-(1/12)\gamma^2 G^2 D\tau^3]$, where $G$ is the field gradient.[4] We ask that at times $\tau < T_2$ this decay effect is not appreciably less than that due to $T_2$ itself, i.e., let $(1/12)\gamma^2 G^2 D\tau^3 > T_2$. These two constraints yield: $D < 12/\gamma^2 G^2 T_2$.[3] For a typical value of $(\gamma T_2)^{-1} \sim 1$ G and of $G \sim 100$ G/cm, then $D > 2 \times 10^4$ cm$^2$/s. More ideal, yet realizable conditions would be $(\gamma T_2)^{-1} \sim 0.1$ G and $G \sim 10^3$ G/cm, so that $D > 2 \times 10^{-1}$ cm$^2$/s, which is still too large a lower limit.
[43] Thus, for example, in Ref. 10, the HSE results lead to estimates for TEMPONE in the isotropic and nematic phases of **40,6** of $D = 2.2 \times 10^{-6}$ (363 K) and $1.4 \times 10^{-6}$ cm$^2$/s (333 K), respectively.
[44] This result is also found by optimizing, with respect to $B'$, the time rate of change of the log of the signal (squared) obtained at resonance.